Prompt Fission Neutron Spectra for Neutron-Induced Fission of ^{239}Pu and ^{235}U

Matthew Devlin[1,*], *Jaime A.* Gomez[1], *Keegan J.* Kelly[1], *John M.* O'Donnell[1], *Robert C.* Haight[1], *Terry N.* Taddeucci[1], *Denise* Neudecker[1], *Ching-Yen* Wu[2], *Jack* Henderson[2], *Morgan C.* White[1], *Brian* Bucher[2], *Matthew Q.* Buckner[2], *Hye Young* Lee[1], *Shea M.* Mosby[1], *John L.* Ullmann[1], *Nikolaos* Fotiades[1], and *Roger A.* Henderson[2]

[1]Los Alamos National Laboratory, Los Alamos, NM 87545 USA
[2]Lawrence Livermore National Laboratory, Livermore, CA 94550 USA

Abstract. We report the current results of a large effort to accurately measure the Prompt Fission Neutron Spectra (PFNS) for neutron-induced fission of ^{235}U and ^{239}Pu for incident neutrons with energies from 1 to 20 MeV. The Chi-Nu experiment at the Los Alamos Neutron Science Center used an unmoderated, white spectrum of neutrons to induce fission in actinide samples that were placed inside a parallel plate avalanche counter to provide a fast fission signal. A double time-of-flight technique was used to determine the incoming and outgoing neutron energies. Two neutron detector arrays, one with 54 liquid scintillators and another with 22 lithium glass detectors, were used to detect the outgoing neutrons and measure the PFNS distributions over a wide range in outgoing neutron energy, from below 100 keV to 10 MeV. Extensive Monte Carlo modeling was used to understand the experiment response and extract the PFNS. Systematic errors and uncertainties in the method have been examined and quantified. A summary of these results for incoming energies from 1 to 5 MeV is presented here.

1 Introduction

Prompt Fission Neutron Spectra (PFNS) measurements for neutron-induced fission have been of interest since shortly after the discovery of fission [1]. Early attempts at such measurements were necessarily primitive, but interest in these spectra was such that the first numbered report from the then secret program at Los Alamos was titled *A Discussion of the Fission Neutron Spectrum* [2]; this document is no longer classified. More recently, there has been a renewed interest in improved PFNS data, with numerous experimental efforts (see, for example, [3–11]) and related evaluations [12–14] for neutron-induced fission of the major actinides. Improved data on PFNS are needed, particularly for fast neutrons, to improve nuclear data libraries [15, 16] used in neutronics calculations for fast systems. These data needs were listed in the recent CIELO nuclear data program [17, 18] of high-priority measurements and evaluations. In addition, improved PFNS data are useful as a test for fission models.

In this paper we present measurements of the PFNS for multiple incident neutron energy ranges from 1 – 5 MeV following neutron-induced fission of ^{235}U and ^{239}Pu. These measurements were made as part of the "Chi-Nu" project, and the experiments have been partially described previously in, for example, Refs. [19–21]. Preliminary results, particularly for the lower-energy part of the PFNS for ^{235}U, have also been reported previously; the results reported here are of a less preliminary nature, and should supersede the prior reported values. These newer results include a large fraction of the PFNS, for fast neutron-induced fission of both ^{235}U and ^{239}Pu. Pre-equilibrium neutron distributions in the fission of ^{239}Pu have been reported previously [22], and these features as well as other features in the PFNS for incoming neutron energies above 5 MeV are reported elsewhere in this volume [23].

2 Experiments and Analysis

The Chi-Nu experiments use a broad spectrum of neutrons produced at the The Los Alamos Neutron Science Center (LANSCE) and a double time-of-flight technique to determine the incoming and outgoing neutron energies. The LANSCE linear accelerator uses an 800 MeV proton beam to generate neutrons by proton-induced spallation on a tungsten target [24]. The LANSCE proton beam is delivered to various facilities, including the Weapons Neutron Research facility (WNR). Protons are delivered in "macropulses" at a rate of 120 Hz, with WNR receiving typically five out of six of these macropulses. Each of these macropulses consists of numerous "micropulses," with sub-nanosecond proton beam timing, separated by typically ≈ 1.8 μs. WNR uses an unmoderated tungsten target, and the resulting useful neutron beams consist of neutrons from below 1 MeV up to over 700 MeV. Slow neutrons from preceding micropulses can reach the samples, and this effect is referred to as "wraparound." Chi-

*e-mail: devlin@lanl.gov

Nu uses a beam line at 15 degrees from the proton beam direction, with a target position of approximately 21.5 m.

In order to detect fission, approximately 100 mg of ^{235}U or ^{239}Pu is housed in a multi-foil Parallel-Plate Avalanche Counter (PPAC) [25]. The PPAC is made of 10 independent sections that are arranged perpendicular to the direction of the beam. Each section consists of several layers, the first and last layer are platinum separation layers, in between which are aluminum-coated mylar anodes, and in the middle of the stack is the actinide sample on a titanium backing acting as a cathode, with -375 V typically applied. Isobutane gas is continuously flowing through the PPAC and maintained at an approximate internal pressure of 4.2 Torr, with a flow rate between 10 and 20 cc/s. Fission fragments produce an electron avalanche in the PPAC, identifying a fission event, and providing a fission signal time. In addition, an identical PPAC with the spontaneously fissioning isotope ^{252}Cf was used to validate the modeling described later. Only one cell was used for this PPAC, but all other features including the housing, gas supply, and support structures were identical.

The PPAC is positioned at a distance of 106.7 cm above an 18 ft x 18 ft thin aluminum floor. Detection of a fission fragment in a PPAC cell provides a stop signal for the incoming neutron, whose start signal is provided by the proton beam just prior to a micropulse striking the neutron production target. This fission detection also provides a start signal for the TOF measurement of the outgoing fission neutrons; since both the incident and outgoing neutron energies are determined by TOF, this techniques has been referred to as a "double time-of-flight" method. The outgoing neutrons are then detected in one of two arrays: an array of 22 Li glass scintillation ("'Li-glass") detectors used for measuring the low energy region of the PFNS (10 keV – 1.5 MeV) and, in separate experiments, an array of 54 liquid organic scintillators (EJ309) for the high energy region (850 keV and above). Twenty-one of the Li glass detectors are enriched with ^{6}Li, while one is enriched with ^{7}Li. Each set of detectors is held in place by a rigid frame, with the front of the Li glass detectors at a distance of 40 cm from the center of the PPAC, and the liquid scintillators at a distance of 1.0 m from the center. Fig. 1 shows a rendering of the liquid scintillator array. The Li glass array identifies neutrons using the signals from the ^{6}Li(n,α)t reaction, while the liquid scintillator array uses pulse-shape discrimination; kinematic cuts are also used with both arrays to distinguish neutrons from γ-rays.

Signals from all of the detectors, as well as the timing signal from the proton beam, are recorded using an asynchronous readout, which allows for maximum data throughput and minimizes dead-time effects. Once the data are collected, coincidences are reconstructed offline. Random backgrounds, from neutron events not coincident with fission, are measured using the method described in Ref. [26], making use of the singles rates obtained with the asynchronous readout of every channel. The recorded neutron events are used to infer the PFNS distribution using a high-fidelity Monte Carlo model of the experiment using MCNP®6.2 [27] with the PTRAC output format and MCNPX-PoliMi [28, 29]. This model was used to construct a response matrix representing the effect of the experimental environment on neutrons emitted from the fissile targets, as discussed in Refs. [30, 31]. Fig. 2 shows one such response matrix, for the Li glass array.

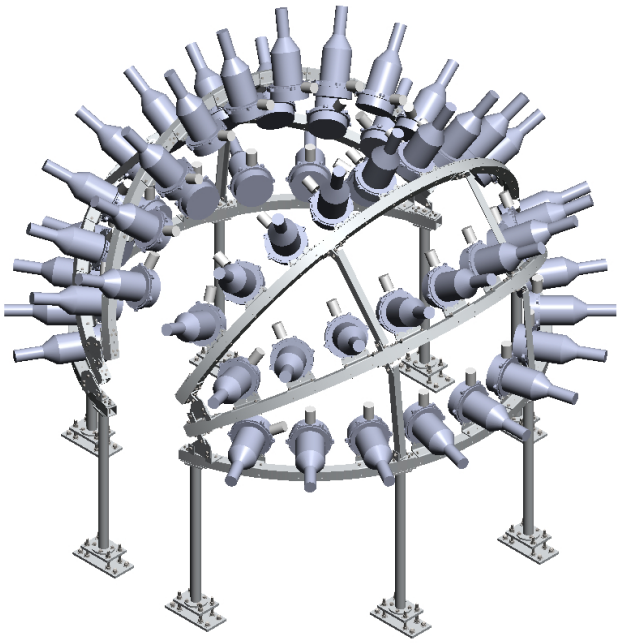

Figure 1. Rendering of the 54-element Chi-Nu liquid scintillator array.

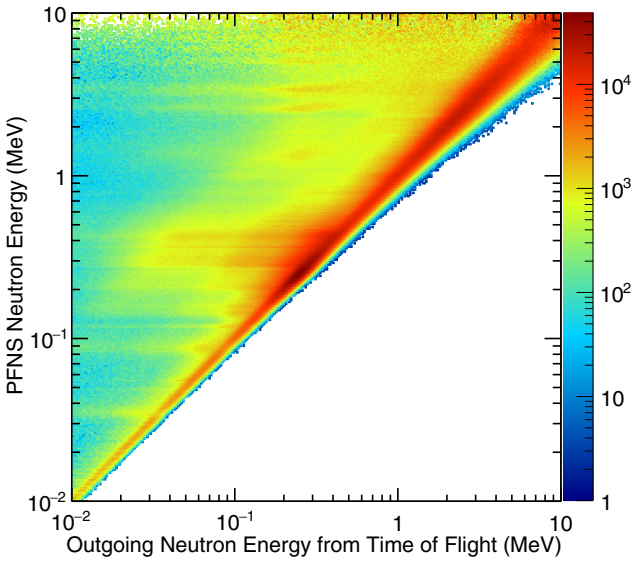

Figure 2. The simulated response matrix for the Li glass array. Neutrons which travel directly to a detector are seen on the diagonal, and scattered neutrons, since they take longer to reach a detector, can be seen above the diagonal. Note the prominant resonance in the ^{6}Li(n,α) cross section at 240 keV.

3 ^{235}U PFNS Results

The measured PFNS for neutrons incident on ^{235}U are presented in Figs. 3 through 7 for different ranges of incident neutron energies from 1.0 to 5.0 MeV, for both detector arrays. The PFNS data are shown as a ratio to a 1.32 MeV Maxwellian, in order to show small differences between the spectra. The relative normalization of the Li glass and liquid scintillator data sets is done by matching the areas under the overlap region, as discussed in Ref. [32]. The data are compared to ENDF/B-VII.1 and VIII.0, and to the data from Ref. [5], in ratio to the same Maxwellian. The shaded bands on the figures represent the uncertainties in ENDF/B-VIII.0 for the energies shown. Note that no CHi-Nu data was used in the ENDF/B-VIII.0 evaluation for the incident neutron energies shown in this paper.

The data of Lestone were obtained with a very different method, one that reanalyzed diagnostic data from a past nuclear weapons test, and as such has an incident neutron distribution similar to the PFNS itself. The measured PFNS for the ^{235}U target is consistent with ENDF/B-VIII.0 within evaluated uncertainties. However, there are consistent excesses of measured mean values over evaluated data at low PFNS energies, perhaps indicating a flatter spectrum. Some excess is also observed at high PFNS energies. Note that the observed excess of low energy neutrons in the PFNS for ^{235}U, compared to the evaluations, is largely within the uncertainty bands of ENDF/B-VIII.0. It is also roughly consistent with the inferred PFNS suggested by V.M. Maslov, *et al.* in Refs. [33, 34].

These data are corrected for most, but not all, known sources of bias. The missing corrections include the effect of wraparound neutrons, which is expected to be below one percent for each energy bin. In addition, corrections for the PPAC angular acceptance (for fission fragments), and fission fragment anisotropies are also not included in these results. These corrections are in the process of being finalized. Additional data were also taken down to 10 keV in outgoing neutron energy, and for incident energies up to 20 MeV.

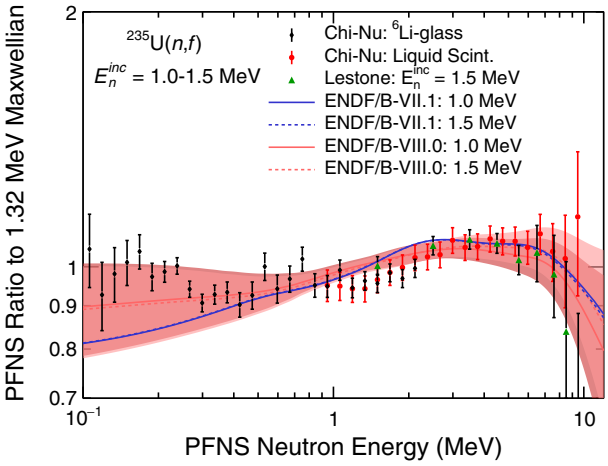

Figure 3. PFNS spectrum for 1.0 – 1.5 MeV neutrons incident on ^{235}U, from both of the Chi-Nu detector arrays (Li glass and Liquid Scintillators), compared to ENDF/B-VII.1 and ENDF/B-VIII.0, and to the data from Ref. [5] (Lestone). The shaded bands represent the uncertainties in ENDF/B-VIII.0 for the energies shown.

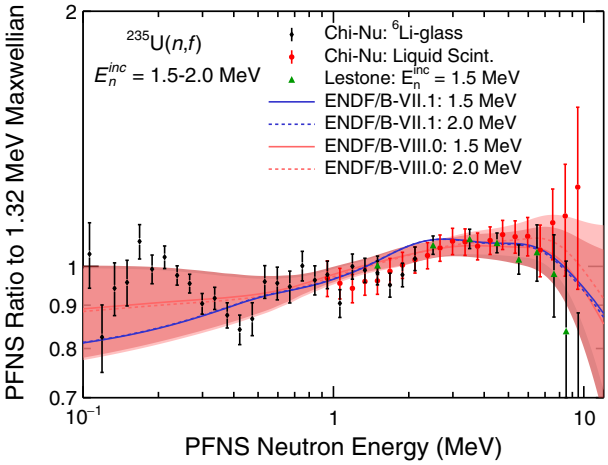

Figure 4. Similar to Fig. 3, with an incident neutron range of 1.5 to 2.0 MeV.

4 ^{239}Pu PFNS Results

The measured PFNS for neutrons incident on ^{239}Pu are presented in Figs. 8 through 11 for different ranges of incident neutron energies between 1.2 and 5.0 MeV, for both detector arrays. The PFNS data are shown as a ratio to a 1.424 MeV Maxwellian. The relative normalization of the Li glass and liquid scintillator data sets is handled in the same manner as in the ^{235}U PFNS data above. The data are compared to ENDF/B-VIII.0, JEFF-3.3 [36], and to the data from Ref. [5] in the same ratio to the Maxwellian. The shaded bands on the figures represent the uncertainties in ENDF/B-VIII.0 and JEFF-3.3 for the energies shown. In Fig. 8, the incident neutron energy range of 1.2 to 1.8 MeV is chosen to match the median energy as closely as possible to that of an incident PFNS spectrum, to provide a direct comparison to the Lestone data.

The measured PFNS for the ^{239}Pu target is consistent with ENDF/B-VIII.0 within evaluated uncertainties. However, there are consistent excesses of measured mean values over evaluated data at low PFNS energies, perhaps indicating a flatter spectrum. There is an observed excess of low energy neutrons in the PFNS for ^{239}Pu, compared to the evaluations, though the uncertainties overlap the uncertainty bands of ENDF/B-VIII.0. Again, this excess is roughly consistent with the inferred PFNS by V.M. Maslov, *et al.* in Refs. [34, 35]. At higher PFNS energies, the new data are generally within the uncertainty bands of ENDF/B-VIII.0. Corrections for the PPAC angular acceptance (for fission fragments), fission fragment anisotropies, and wraparound neutrons are not included in these results. Additional data were also taken down to 10

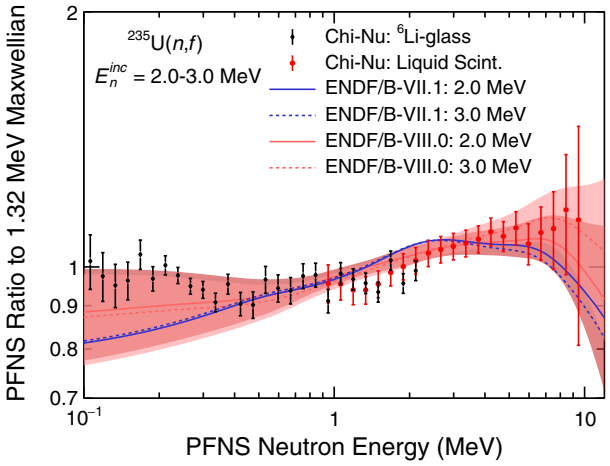

Figure 5. Similar to Fig. 3, with an incident neutron range of 2.0 to 3.0 MeV.

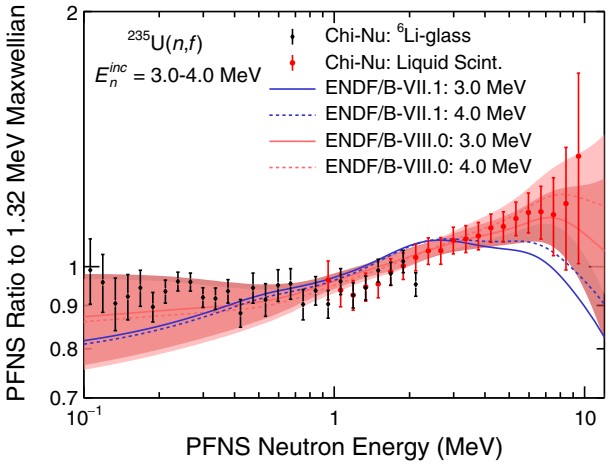

Figure 6. Similar to Fig. 3, with an incident neutron range of 3.0 to 4.0 MeV.

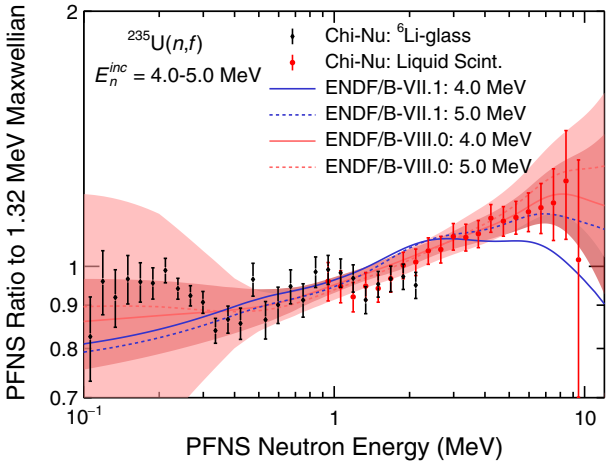

Figure 7. Similar to Fig. 3, with an incident neutron range of 4.0 to 5.0 MeV.

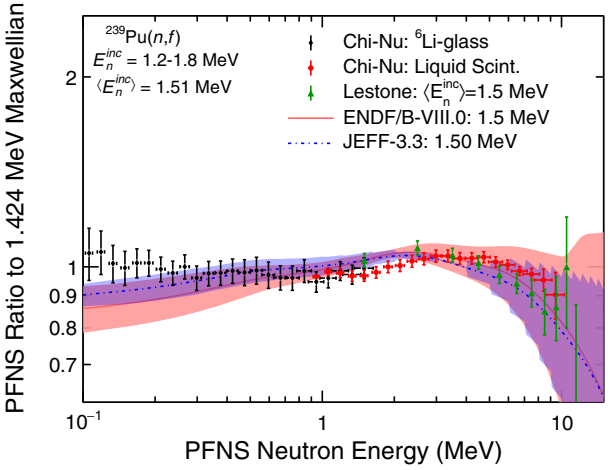

Figure 8. PFNS spectrum for 1.2 – 1.8 MeV neutrons incident on ^{239}Pu, from both of the Chi-Nu detector arrays (^{6}Li glass and Liquid Scintillators), compared to ENDF/B-VIII.0, JEFF-3.3, and to the data from Lestone [5]. The shaded bands represent the uncertainties in ENDF/B-VIII.0 and JEFF-3.3 for the energies shown.

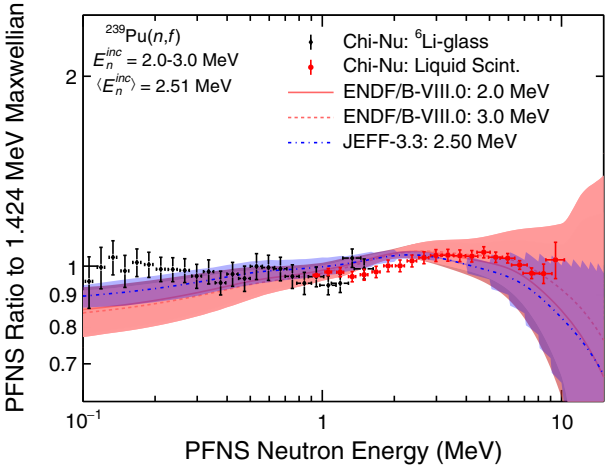

Figure 9. Similar to Fig. 8, with an incident neutron range of 2.0 to 3.0 MeV.

keV in outgoing neutron energy, and for incident energies up to 20 MeV.

5 Uncertainty quantification and correlations

Accurate characterizations of experimental uncertainties are one of the central issues for nuclear data evaluations. The PFNS results reported here include statistical and systematic uncertainties, including a wide variety of systematic effects. These systematic issues range from the effects of the background determination and its uncertainties, the effects of resolutions and other parameters used in the Monte Carlo simulations to compare to the data, and the effects of uncertain nuclear cross sections in the Monte Carlo simulations[37]. Each of these issues gives rise to

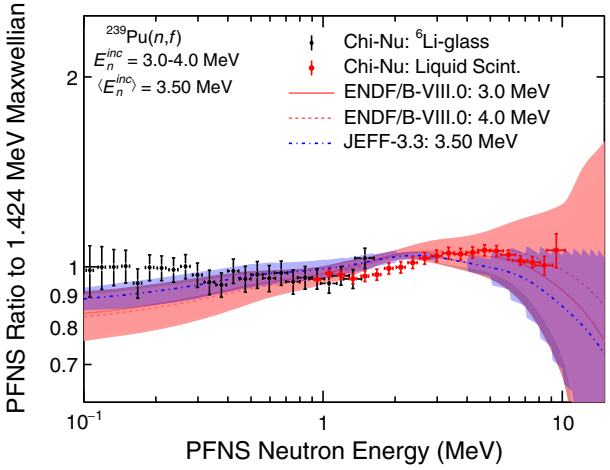

Figure 10. Similar to Fig. 8, with an incident neutron range of 3.0 to 4.0 MeV.

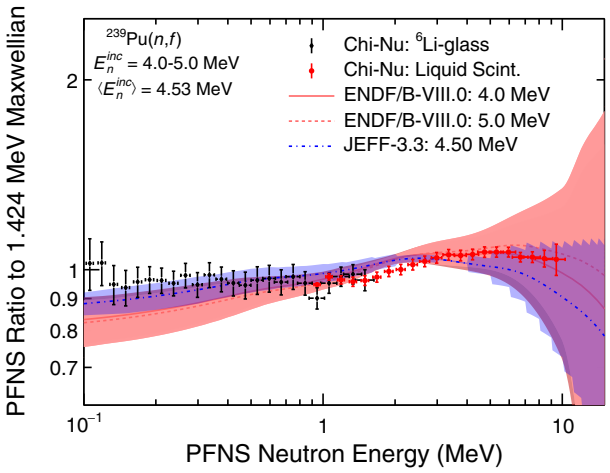

Figure 11. Similar to Fig. 8, with an incident neutron range of 4.0 to 5.0 MeV.

(possibly) a correction to the data, to an additional uncertainty, and to correlations in the uncertainties between data points.

As an example of these analyses, Fig. 12 shows the covariance matrix for these correlations due to the background subtraction within the Li glass dataset for the PFNS data on ^{239}Pu. The background is largest at the lowest PFNS neutron energies, as can be seen in the matrix. In addition, background uncertainties are highly correlated across all energies. As another example, Fig. 13 shows the covariance matrix for correlations from variations in some of the parameters used in the MCNP simulation of the detector array response for the liquid scintillator array. The parameters varied include the pulse height threshold and resolution, which are matched to the experimental values, but which also have uncertainties. Again, the lowest PFNS energies are most affected by threshold effects, in a correlated manner. Note that the darkest areas actually represent negative values. A more detailed discussion of these

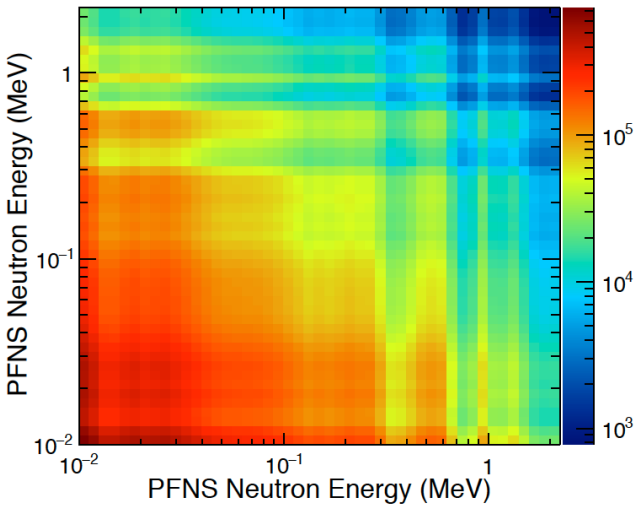

Figure 12. Covariance matrix for the Li glass array PFNS data due to the random background subtraction.

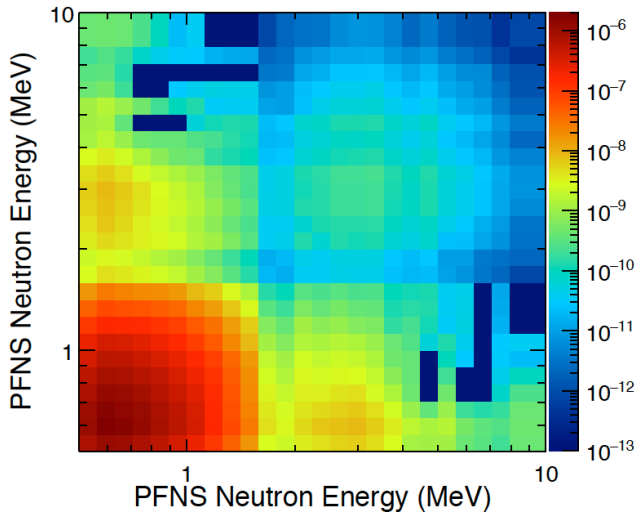

Figure 13. Covariance matrix for the liquid scintillator array PFNS data due to variations in the pulse height threshold and resolution parameters used in the MCNP simulations.

analyses will be presented in a forthcoming paper. Some additional details can also be found in Ref. [32].

6 Summary

Prompt fission neutron spectra for 1 to 5 MeV neutron-induced fission of ^{235}U and ^{239}Pu have been presented. These data agree reasonably well with ENDF/B evaluations. Final results and a complete discussion of the systematic uncertainties and their correlations will be provided in upcoming publications.

Acknowledgements

This work was supported by the US Department of Energy through the Los Alamos National Laboratory and

Lawrence Livermore National Laboratory. Los Alamos National Laboratory is operated by Triad National Security, LLC, for the National Nuclear Security Administration of U.S. Department of Energy under Contract No. 89233218CNA000001. Lawrence Livermore National Laboratory is operated under Contract DE-AC52-07NA27344. These experiments benefited from the use of neutrons at the Los Alamos Neutron Science Center.

References

[1] O. Hahn and F. Strassmann, Naturwissenschaften **27**, 11 (1939).

[2] W.E. Bennett and H.T. Richards, "A Discussion of the Fission Neutron Spectrum," Los Alamos National Laboratory Report, LA-MS-1, 1943.

[3] A. Enqvist, B.M. Wieger, L. Huang, *et al.*, Phys. Rev. **C 86**, 064605 (2012).

[4] A. Sardet, T. Granier, B. Laurent, and A. Oberstedt, Physics Procedia **47**, 144 (2013).

[5] J.P. Lestone and E.F. Shores, Nucl. Data Sheets **119**, 213 (2014).

[6] V.V. Desai, B.K. Nayak, A. Saxena, S.V. Suryanarayana, and R. Capote, Phys. Rev. **C 92**, 014609 (2015).

[7] Benoit Laurent, Paola Marini, Gilbert Bélier, *et al.* EPJ Web of Conferences **146**, 04014 (2017).

[8] Paola Marini, *et al.*, EPJ Web of Conferences **193**, 03002 (2018).

[9] Tie He, Pu Zheng, and Jun Xiao, Nucl. Science and Techiques **30**, 112 (2019).

[10] S. Noda, R.C. Haight, R.O. Nelson, *et al.*, Phys. Rev. C **83**, 034604 (2011).

[11] A. Chatillon, G. Bélier, T. Granier, *et al.*, Phys. Rev. C **89**, 014611 (2014).

[12] R. Capote, Y.-J. Chen, F.-J. Hambsch, *et al.*, Nucl. Data Sheets **131**, 1 (2016).

[13] D. Neudecker, P. Talou, T.N. Taddeucci, *et al.*, Nucl. Data Sheets **123**, 146 (2015).

[14] D. Neudecker, P. Talou, T. Kawano, *et al.*, Nucl. Data Sheets **148**, 293 (2018).

[15] M.B. Chadwick, M.W. Herman, P. Obložinský *et al.*, Nucl. Data Sheets **112**, 2887 (2011).

[16] D.A. Brown, M.B. Chadwick, R. Capote, *et. al.*, Nucl. Data Sheets **148**, 1 (2018).

[17] M.B. Chadwick, E. Dupont, E. Bauge, *et al.*, Nucl. Data Sheets **118**, 1 (2014).

[18] M.B. Chadwick, E. Dupont, E. Bauge *et al.*, EPJ Web of Conferences **146**, 02001 (2017).

[19] R.C. Haight, H.Y. Lee, T.N .Taddeucci, *et al.*,Nucl. Data Sheets **119**, 205 (2014).

[20] H.Y. Lee, T.N. Taddeucci, R.C. Haight, *et al.*,Nucl. Instr. and Meth. **A703**, 213 (2013).

[21] M. Devlin, J.A. Gomez, K.J.Kelly, *et al.*, Nucl. Data Sheets **148**, 322 (2018).

[22] K.J. Kelly, T. Kawano, J.M. O'Donnell, *et al.*, Phys. Rev. Lett. **122**, 072503 (2019).

[23] K.J. Kelly, *et al.*, in these proceedings.

[24] P.W. Lisowski and K.F. Schoenberg, Nucl. Instr. and Meth. **A562**, 910 (2006); also, see lansce.lanl.gov/facilities/wnr/flightpaths/index.php.

[25] C.Y. Wu, R.A. Henderson, R.C. Haight, *et al.*, Nucl. Instr. and Meth. **A794**, 76 (2015).

[26] J.M. O'Donnell, Nucl. Instr. and Meth. **A805**, 87 (2016).

[27] X-5 Monte Carlo Team, LA-UR-03-1987; Forrest Brown, Brian Kiedrowski, and Jeffrey Bull, "MCNP5-1.60 Release Notes", LA-UR-10-06235 (2010); and https://mcnp.lanl.gov.

[28] S.A. Pozzi, E. Padovani, and M. Marsequerra, Nucl. Instr. and Meth. **A513**, 550 (2003).

[29] S.A. Pozzi, S.D. Clarke, W.J. Walsh, *et al.*, Nucl. Instr. and Meth. **A694**, 119 (2012).

[30] K.J. Kelly, J.M. O'Donnell, J.A. Gomez, *et al.*, Nucl. Instr. and Meth. **A866**, 182 (2017).

[31] T.N. Taddeucci, R.C. Haight, H.Y. Lee, *et al.*, Nucl. Data Sheets, **123**,135 (2015).

[32] K.J. Kelly, J.M. O'Donnell, D. Neudecker, *et al.*, Nucl. Instr. and Meth. **A**., in press, 162449, (2019); https://doi.org/10.1016/j.nima.2019.162449.

[33] V.M. Maslov, *et al.*, Atomic Energy **108**, 432 (2010).

[34] V.M. Maslov, *et al.*, J. of the Korean Phys. Soc. **59**, 1337 (2011).

[35] V.M. Maslov, Atomic Energy **103**, 633 (2007).

[36] See https://www.oecd-nea.org/dbdata/jeff/.

[37] K.J. Kelly, et al., Nucl. Inst. and Meth. **A** (2018), in press; https://doi.org/10.1016/j.nima.2018.10.089.